J. Fluid Mech. (2006), *vol.* 557, *pp.* 237–256.
doi:10.1017/S0022112006009773 Printed in the United Kingdom

On gravity–capillary lumps. Part 2. Two-dimensional Benjamin equation

By BOGUK KIM[1] AND T. R. AKYLAS[2]

[1]Department of Mathematics, Massachusetts Institute of Technology, Cambridge, MA 02139, USA
[2]Department of Mechanical Engineering, Massachusetts Institute of Technology, Cambridge, MA 02139, USA

(Received 25 January 2005 and in revised form 28 November 2005)

A theoretical study is made of fully localized solitary waves, commonly referred to as 'lumps', on the interface of a two-layer fluid system in the case that the upper layer is bounded by a rigid lid and lies on top of an infinitely deep fluid. The analysis is based on an extension, that allows for weak transverse variations, of the equation derived by Benjamin (*J. Fluid Mech.* vol. 245, 1992, p. 401) for the evolution in one spatial dimension of weakly nonlinear long waves in this flow configuration, assuming that interfacial tension is large and the two fluid densities are nearly equal. The phase speed of the Benjamin equation features a minimum at a finite wavenumber where plane solitary waves are known to bifurcate from infinitesimal sinusoidal wavetrains. Using small-amplitude expansions, it is shown that this minimum is also the bifurcation point of lumps akin to the free-surface gravity–capillary lumps recently found on water of finite depth. Numerical continuation of the two symmetric lump-solution branches that bifurcate there reveals that the elevation-wave branch is directly connected to the familiar lump solutions of the Kadomtsev–Petviashvili equation, while the depression-wave branch apparently features a sequence of limit points associated with multi-modal lumps. Plane solitary waves of elevation, although stable in one dimension, are unstable to transverse perturbations, and there is evidence from unsteady numerical simulations that this instability results in the formation of elevation lumps.

1. Introduction

In contrast to plane solitary waves, which are ubiquitous, fully localized solitary waves arise under rather special flow conditions. This apparently accounts for the fact that such so-called lumps have received far less attention than plane solitary waves.

The majority of prior work deals with lumps in the weakly nonlinear long-wave limit and is based on the Kadomtsev–Petviashvili (KP) equation, an extension of the Korteweg–de Vries (KdV) equation that allows for weak spatial variations transverse to the propagation direction (see, for example, Akylas 1994). While the KdV equation predicts that plane solitary waves are always possible, the KP equation admits lump solutions only if the linear-long-wave speed happens to be a minimum of the phase speed, and this property is met under very restricted flow conditions. In the classical water-wave problem, in particular, lumps of the KP type are possible only in the high-surface-tension regime (Bond number greater than 1/3), which requires the fluid depth to be less than a few mm (see, for example, Ablowitz & Segur 1979).

In Part 1 (Kim & Akylas 2005), however, it was pointed out that gravity–capillary lumps of a different kind can in fact be found on water of finite or infinite depth for Bond number less than 1/3. Rather than the long-wave speed, these lumps bifurcate from a linear sinusoidal wavetrain with finite wavenumber at the minimum of the gravity–capillary phase speed, and are fully localized counterparts of the plane solitary waves that are known to bifurcate there (Dias & Iooss 1993; Akylas 1993; Longuet-Higgins 1993). Based on weakly nonlinear expansions close to the bifurcation point, it was shown in Part 1 that small-amplitude lumps take the form of locally confined modulated wavepackets with carrier oscillations that are stationary relative to the envelope. In water of finite depth, in particular, the wave envelope and the induced mean flow are governed by an elliptic–elliptic Davey–Stewartson equation system, and lumps always feature algebraically decaying tails owing to this mean flow. Although in Part 1 the discussion focused on gravity–capillary water waves, a similar local analysis would apply in general close to an extremum of the phase speed at a finite wavenumber, suggesting that lumps of the same type could be found in other instances as well.

In closely related numerical work, Parau, Vanden-Broeck & Cooker (2005) recently computed gravity–capillary lumps in deep water that, indeed, resemble fully localized wavepackets in the small-amplitude limit close to the minimum phase speed. Also, based on a weakly nonlinear model, Milewski (2005) was able to connect, via numerical continuation, lumps of the KP equation in shallow water to lumps of the wavepacket type near the minimum gravity–capillary phase speed in water of finite depth. The asymptotic and numerical results, moreover, are supported by a rigorous existence proof of fully localized gravity–capillary solitary waves, recently devised by Groves & Sun (2005).

These findings have firmly estabilished that free-surface gravity–capillary lumps are possible under quite general flow conditions. On the other hand, the stability of the computed steady-solution branches, as well as the feasibility of obtaining lumps from general locally confined initial conditions, remain unexplored. These issues are of paramount importance in assessing the relevance of the new class of lumps from a physical viewpoint.

In regard to the question of stability, it is worth noting that, in the small-amplitude limit where lumps behave like wavepackets, the elliptic–elliptic Davey–Stewartson equations predict focusing of the wavepacket envelope at a finite time, for initial conditions above a certain threshold (Ablowitz & Segur 1979; Papanicolaou *et al.* 1994). Given that lumps may be viewed as modulated wavepackets only in the vicinity of the bifurcation point, however, it is not clear to what extent they are affected by this nonlinear-focusing instability.

In the present paper, we make a first step towards settling some of these open questions. For simplicity, rather than the full water-wave equations, we shall work with a model equation for interfacial gravity–capillary waves; namely, we consider an extension to two spatial dimensions of the evolution equation derived by Benjamin (1992) for weakly nonlinear long waves on the interface of a two-fluid system, in the case that the upper layer is bounded by a rigid lid and lies on top of an infinitely deep fluid.

In this flow configuration, when interfacial tension is assumed to be large and the two fluid densities are nearly equal, the KdV and the Benjamin–Davis–Ono (BDO) dispersive terms for long interfacial waves become equally important. As a result, the phase speed of the Benjamin equation features a minimum at a finite wavenumber, which is the bifurcation point of plane solitary waves akin to the free-surface solitary

waves bifurcating at the minimum gravity–capillary phase speed (Akylas, Dias & Grimshaw 1998; Albert, Bona & Restrepo 1999; Calvo & Akylas 2003).

Accounting for transverse spatial variations, the resulting long-wave equation combines the KdV and BDO dispersive terms with the transverse spatial term of the KP equation. This two-dimensional Benjamin (2-DB) equation admits lumps, which again bifurcate at the minimum phase speed, and in the small-amplitude limit are analogous to the free-surface lumps on water of finite depth found in Part 1. Numerical continuation in the finite-amplitude regime reveals that lumps of elevation are directly connected to lumps of the KP type in the KdV limit, while lumps of depression apparently undergo successive limit-point bifurcations associated with the appearance of multi-modal lumps.

According to the 2-DB equation, plane solitary waves are unstable to transverse perturbations. Numerical simulations indicate that this instability results in the formation of elevation lumps, which appear to propagate stably, thus assuming the role of asymptotic states of the initial-value problem in two spatial dimensions.

Unfortunately, it becomes prohibitively expensive to extend our simulations very close to the bifurcation point, as lumps decay slowly at infinity in this limit, and we have not been able to study in any systematic way the effect of the nonlinear focusing predicted by the Davey–Stewartson equations on the propagation of lumps. Nevertheless, we have seen no evidence of this type of instability in the computations discussed here.

As discussed in Calvo & Akylas (2003), while the Benjamin equation is formally valid in a very specific flow regime, it remains reliable qualitatively for a wide range of flow conditions, making the generation of this type of interfacial solitary wave feasible experimentally. It is likely that this is the case as well for the 2-DB equation and its lump solutions.

2. Preliminaries

Consider a fluid layer of depth h and density ρ_2 that is bounded above by a rigid lid and lies on top of an infinitely deep fluid of density $\rho_1 > \rho_2$.

The Benjamin equation governs the propagation of straight-crested uni-directional weakly nonlinear long waves on the interface of this two-fluid system, ignoring the effects of viscosity and assuming that interfacial tension is large and the fluid densities are nearly equal (Benjamin 1992). Under these flow conditions, the 2-DB equation is an extension of the Benjamin equation that allows for weak spatial variations transverse to the propagation direction, and can be derived by a standard weakly nonlinear long-wave expansion (see Kim 2006). Here, however, in the interest of brevity, we sketch a heuristic derivation based on the linear dispersion relation.

In dimensionless variables, using h as lengthscale and $(gh)^{1/2}$ as velocity scale, the linear dispersion relation of interfacial waves with wavenumber κ and frequency ω has the following expansion in the long-wave limit ($\kappa \to 0$):

$$\omega = \pm c_0 \kappa \left(1 - \frac{|\kappa|}{R} + \frac{W}{2}\kappa^2 + \cdots \right), \tag{2.1}$$

where

$$R = \frac{\rho_1}{\rho_2}, \quad W = \frac{T}{\delta \rho g h^2}, \quad c_0 = \frac{1-R}{R}, \tag{2.2}$$

T being the interfacial tension, g the gravitational acceleration and $\delta\rho = \rho_1 - \rho_2$ the density difference of the two fluids.

According to (2.1), to leading order, long waves are non-dispersive and propagate with speed $\pm c_0$; the first effects of dispersion normally derive from the term proportional to $\kappa|\kappa|$ in (2.1) which translates into a dispersive term of the BDO type in the corresponding long-wave evolution equation. In the flow regime considered by Benjamin (1992), $W \gg 1$, however, the next-order correction, proportional to κ^3, becomes equally important, in which case a KdV dispersive term comes into play as well; in this instance, the propagation of weakly nonlinear long interfacial waves in one spatial dimension is then governed by the Benjamin equation.

To allow for weak transverse variations, returning to (2.1), we use the fact that uni-directional nearly plane waves with wavenumber

$$\kappa = (k^2 + m^2)^{1/2} = k + \frac{1}{2}\frac{m^2}{k} + \cdots, \tag{2.3}$$

k being the wavenumber component along the propagation (x-, say) direction and $m \ll k$ the wavenumber component in the transverse (z-, say) direction, obey the dispersion relation

$$\omega = c_0 k - \frac{c_0}{2R} k|k| + \frac{c_0}{2} W k^3 + \frac{c_0}{2}\frac{m^2}{k}, \tag{2.4}$$

including the leading-order dispersive and transverse-variation effects. Based on (2.4), as each term corresponds to a specific linear operator in the real domain,

$$\omega \leftrightarrow \mathrm{i}\frac{\partial}{\partial t}, \quad k \leftrightarrow -\mathrm{i}\frac{\partial}{\partial x}, \quad m \leftrightarrow -\mathrm{i}\frac{\partial}{\partial z}, \quad |k| \leftrightarrow -\frac{\partial}{\partial x}\mathscr{H}, \tag{2.5}$$

one can read off the linear terms of the 2-DB equation; upon adding the familiar KdV-type quadratic nonlinear term, the full evolution equation for the interfacial elevation $y = \eta(x, z, t)$ in a reference frame moving with the long-wave speed c_0,

$$x \to x - c_0 t, \tag{2.6}$$

then turns out to be

$$\left(\eta_t + \frac{3}{2} c_0 \eta\eta_x + \frac{c_0}{2R}\mathscr{H}\{\eta_{xx}\} - \frac{c_0}{2} W \eta_{xxx}\right)_x + \frac{c_0}{2}\eta_{zz} = 0, \tag{2.7}$$

where $\mathscr{H}$ stands for the Hilbert transform with respect to x:

$$\mathscr{H}\{f\} = \frac{1}{\pi} \int_{-\infty}^{\infty} \frac{f(\xi)}{\xi - x}\, \mathrm{d}\xi. \tag{2.8}$$

As expected, the 2-DB equation (2.7) combines the KdV and BDO dispersive terms with the transverse-variation term of the KP equation. In the absense of the BDO term, since the KdV dispersive term and the transverse-variation term have opposite signs, (2.7) reduces to the so-called KP-I equation that governs shallow-water waves in the high-surface-tension regime (Bond number greater than 1/3). In the other extreme, when the KdV dispersive term is ignored, (2.7) reduces to the two-dimensional BDO equation derived by Ablowitz & Segur (1980) for internal waves in stratified fluids of large depth.

Locally confined solutions of the 2-DB equation (2.7) are subject to the constraint

$$\int_{-\infty}^{\infty} \eta(x, z, t)\, \mathrm{d}x = 0, \tag{2.9}$$

that also applies to the KP and the two-dimensional BDO equations. As explained in Katsis & Akylas (1987), this constraint derives from considering nearly plane

wave disturbances with weak transverse variations: it is clear from (2.3) that Fourier components with $k=0$ and $m \neq 0$ violate this assumption, and the constraint (2.9) simply ensures that no such wave components are present in the disturbance. For detailed discussions of this constraint in connection with the initial-value problem of the KP equation, see Grimshaw & Melville (1989) and Ablowitz & Wang (1997).

It is also worth noting that, in contrast to the full interfacial-wave equations, the 2-DB equation is not isotropic, as it describes nearly uni-directional waves, x thus being a preferred direction. This might seem to suggest that possible lump solutions of this model equation depend on the direction of propagation, casting doubt on their physical relevance. As discussed below, however, oblique lump solutions can in fact be mapped to lumps propagating along the x-direction via a coordinate and speed transformation. Moreover, within the approximations inherent in the derivation of the 2-DB equation, this transformation can be interpreted as merely a rotation of axes.

Specifically, according to (2.7), the profile of an oblique lump $\eta(\xi, \zeta)$ propagating with speed V, say, at an angle ϕ to the x-direction,

$$\xi = x - Vt\cos\phi, \quad \zeta = z - Vt\sin\phi, \tag{2.10}$$

must satisfy

$$\left(-V\cos\phi\ \eta_\xi - V\sin\phi\ \eta_\zeta + \frac{3}{2}c_0\eta\eta_\xi + \frac{c_0}{2R}\mathscr{H}\{\eta_{\xi\xi}\} - \frac{c_0}{2}W\eta_{\xi\xi\xi}\right)_\xi + \frac{c_0}{2}\eta_{\zeta\zeta} = 0. \tag{2.11}$$

By introducing the coordinate transformation

$$\tilde{\xi} = \xi + \frac{V}{c_0}\sin\phi\ \zeta, \quad \tilde{\zeta} = \zeta, \tag{2.12}$$

however, (2.11) can be reduced to the equation satisfied by a non-oblique lump:

$$\left(-\tilde{V}\eta + \frac{3}{4}c_0\eta^2 + \frac{c_0}{2R}\mathscr{H}\{\eta_{\tilde{\xi}}\} - \frac{c_0}{2}W\eta_{\tilde{\xi}\tilde{\xi}\tilde{\xi}}\right)_{\tilde{\xi}\tilde{\xi}\tilde{\xi}} + \frac{c_0}{2}\eta_{\tilde{\zeta}\tilde{\zeta}} = 0, \tag{2.13}$$

with speed

$$\tilde{V} = V\cos\phi + \frac{V^2}{2c_0}\sin^2\phi. \tag{2.14}$$

Hence, any oblique lump solution can be related to a non-oblique lump solution having a different speed given by (2.14).

To interpret the speed transformation (2.14), note that a lump solution of the 2-DB equation (2.7) propagating along the x-axis with speed $\tilde{V}$, say, in fact would move with speed $c_0 + \tilde{V}$ in still fluids, in view of the change of reference frame (2.6) which is equivalent to superposing a steady stream $-c_0$ in the x-direction; furthermore, $\tilde{V}/c_0 \ll 1$, since dispersive and nonlinear effects are taken to be weak in deriving the 2-DB equation. Suppose now that the same lump is slightly rotated so that, in still fluids, it propagates at an angle $\alpha \ll 1$ to the x-axis again with speed $c_0 + \tilde{V}$. When viewed from the moving reference frame (2.6), however, the x- and z- velocity components of this lump would be

$$V_x \approx \tilde{V} - \frac{c_0}{2}\alpha^2, \quad V_z \approx \alpha c_0. \tag{2.15}$$

Hence, relative to the moving reference frame, the lump appears to propagate at an angle ϕ to the x-axis with a speed V, where

$$V\cos\phi = \tilde{V} - \frac{c_0}{2}\alpha^2, \quad V\sin\phi = \alpha c_0. \tag{2.16}$$

Note that, according to (2.16), $\tilde{V}$ is related to V precisely as in (2.14) and, moreover, in the coordinate transformation (2.12), $V\sin\phi/c_0$ is equal to the rotation angle α. This confirms that oblique-lump solutions of the 2-DB equation correspond to slightly rotated non-oblique lumps, and in the following attention is focused solely on lumps propagating along x.

In preparation for the ensuing analysis, we re-scale variables according to

$$(x, z) = \frac{1}{W^{1/2}}(x', z'), \quad t' = -\frac{c_0}{2W^{1/2}}t, \quad \eta' = \frac{3}{2}\eta, \tag{2.17}$$

so, after dropping the primes, the 2-DB equation (2.7) takes the normalized form

$$(\eta_t + (\eta^2)_x - 2\gamma\mathscr{H}\{\eta_{xx}\} + \eta_{xxx})_x - \eta_{zz} = 0, \tag{2.18}$$

where

$$\gamma = \frac{1}{2RW^{1/2}}. \tag{2.19}$$

Ignoring transverse variations in (2.18) recovers the Benjamin equation in the form considered in Akylas *et al.* (1998).

3. Steady lumps

For the purpose of computing steady lumps, we shall adhere to the convention adopted in Part 1 and normalize the wave speed to 1. In the reference frame moving with a lump, $\xi = x - t$, the profile $\eta(\xi, z)$ then satisfies a steady version of the 2-DB equation (2.18):

$$(-\eta + \eta^2 - 2\gamma\mathscr{H}\{\eta_\xi\} + \eta_{\xi\xi})_{\xi\xi} - \eta_{zz} = 0, \tag{3.1}$$

and lump-solution branches are traced by varying the parameter γ.

3.1. *Bifurcation of lumps*

As already remarked, in general, lumps bifurcate from infinitesimal-amplitude sinusoidal wavetrains at specific wavenumber k_0 where the phase speed attains an extremum and is thus equal to the group speed. In the normalization used here, it is easy to check that the phase speed of the 2-DB equation (2.18) has a maximum equal to 1 at $k_0 = 1$, for $\gamma = \gamma_0 = 1$. (In view of the time reversal in (2.17), this maximum corresponds to a minimum of the phase speed of the unscaled equation (2.7).)

Close to this bifurcation point, small-amplitude lumps may be viewed as locally confined wavepackets with carrier oscillations that are stationary relative to the wavepacket envelope, and can be described by a multiple-scale expansion. Here we shall only outline the salient features of this weakly nonlinear analysis, as it closely parallels the one presented in Part 1 for free-surface lumps.

In the vicinity of $\gamma_0 = 1$, we write

$$\gamma = 1 - \tfrac{1}{2}\epsilon^2 \quad (\epsilon \ll 1), \tag{3.2}$$

and expand $\eta(\xi, z)$ as follows:

$$\eta = \tfrac{1}{2}\epsilon\{A(X, Z)\mathrm{e}^{\mathrm{i}\xi} + \text{c.c.}\} + \epsilon^2\{A_2(X, Z)\mathrm{e}^{2\mathrm{i}\xi} + \text{c.c.}\} + \epsilon^2 A_0(X, Z) + \cdots, \tag{3.3}$$

where $(X, Z) = \epsilon(\xi, z)$ are the 'stretched' envelope variables and c.c. denotes the complex conjugate.

Substituting expansion (3.3) in equation (3.1) and collecting second-harmonic, mean and primary-harmonic terms up to $O(\epsilon^3)$, it is found that the envelope A and the mean term A_0 satisfy the following coupled system:

$$A_{0XX} + A_{0ZZ} = \tfrac{1}{2}(|A|^2)_{XX}, \tag{3.4}$$

$$A_{XX} + A_{ZZ} - A + \tfrac{1}{2}A^2A^* + 2A_0A = 0. \tag{3.5}$$

This system is entirely analogous to the steady elliptic–elliptic Davey–Stewartson equations derived in Part 1 for the primary-harmonic envelope and the induced mean flow of small-amplitude gravity–capillary lumps on water of finite depth.

To ensure that lump solutions of the 2-DB equation (3.1) are possible, it is necessary to find locally confined solutions of the equation system (3.4) and (3.5). As no such solutions are known in closed form, this system is solved numerically by a continuation procedure suggested in Papanicolaou *et al.* (1994). For this purpose, the factor $\frac{1}{2}$ on the right-hand side of (3.4) is temporarily replaced with ν, say,

$$A_{0XX} + A_{0ZZ} = \nu(|A|^2)_{XX}, \tag{3.6}$$

which serves as the continuation parameter in tracking solutions of the equation system (3.5) and (3.6).

From (3.6), $A_0 \to 0$ as $\nu \to 0$ so, in this limit, the coupling of A to A_0 vanishes, and (3.5) reduces to a steady two-dimensional nonlinear Schrödinger equation:

$$A_{XX} + A_{ZZ} - A + \tfrac{1}{2}A^2A^* = 0. \tag{3.7}$$

As discussed in Part 1, (3.7) admits radially symmetric locally confined solutions, $A(r)$, where $r^2 = X^2 + Z^2$, that satisfy the boundary-value problem

$$\frac{\mathrm{d}^2A}{\mathrm{d}r^2} + \frac{1}{r}\frac{\mathrm{d}A}{\mathrm{d}r} - A + \frac{1}{2}A^3 = 0 \qquad (0 < r < \infty), \tag{3.8}$$

$$\frac{\mathrm{d}A}{\mathrm{d}r} = 0 \qquad (r = 0), \tag{3.9a}$$

$$A \to 0 \qquad (r \to \infty). \tag{3.9b}$$

Working now with the equation system (3.5) and (3.6), by exploiting the fact that A and A_0 uncouple in the limit $\nu \to 0$, a locally confined solution of the Davey–Stewartson equations (3.4) and (3.5), corresponding to a lump, was obtained as follows: starting at $\nu = 0$ with $A_0 = 0$ and the known ground-state solution of the problem (3.8)–(3.9) that decays monotonically to zero, we computed locally confined solutions of (3.5) and (3.6) for $\nu > 0$ by increasing ν incrementally until the desired value of $\nu = \frac{1}{2}$ was reached. As in Part 1, the equations (3.5) and (3.6) were discretized by a pseudospectral method combined with mapping the (X, Z)-plane into a bounded square domain. For each value of ν, the corresponding nonlinear algebraic equations were solved by Newton's method in only one quarter of the domain, taking advantage of symmetry, and using the known solution at the previous value of ν as first guess (see Kim 2006 for details).

Figure 1 shows X- and Z-cross-sections of the computed profiles $A(X, Z)$ and $A_0(X, Z)$. The maximum of A, which corresponds to the lump peak amplitude, occurs at the origin $X = Z = 0$. Also, it is seen that the mean term A_0 decays at infinity more slowly than the primary-harmonic envelope A and, as it turns out, controls the behaviour at the tails of lumps.

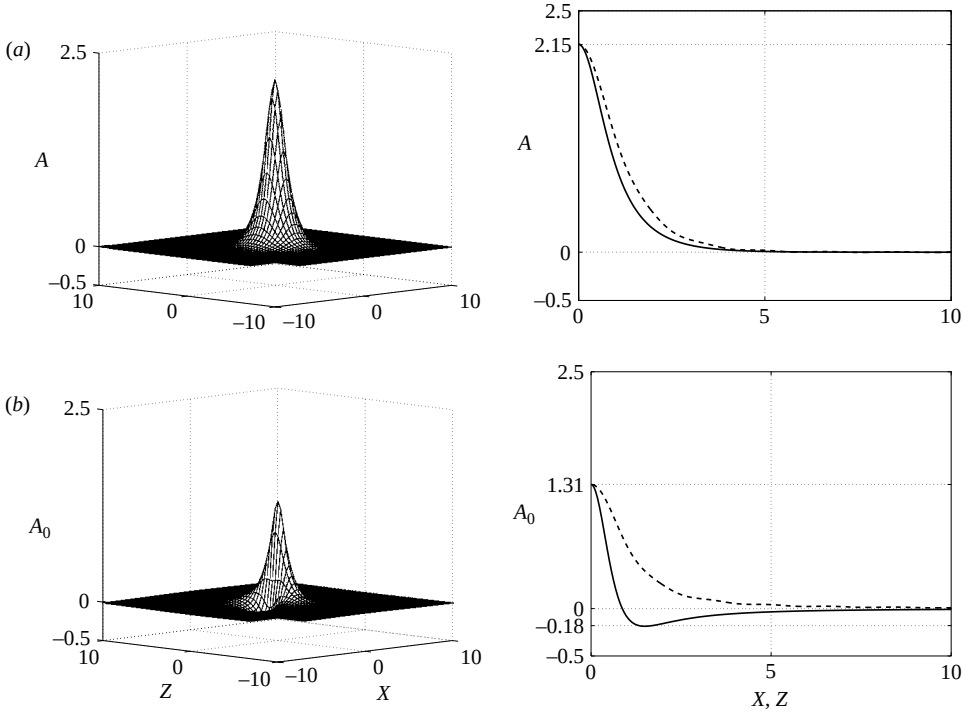

FIGURE 1. Locally confined solution of the Davey–Stewartson equations (3.4) and (3.5). (*a*) Primary-harmonic envelope A; (*b*) mean term A_0. X-cross-section (–); Z-cross-section (- -).

Specifically, from (3.5), A decays exponentially, $A \propto \exp(-r)$ as $r \to \infty$. On the other hand, upon taking the Fourier transform with respect to X and Z, it follows from (3.4) that

$$A_0 \sim -\frac{I_0}{4\pi}\frac{\partial}{\partial Z}\left(\frac{Z}{X^2+Z^2}\right) \qquad (r \to \infty), \tag{3.10}$$

where

$$I_0 = \int_{-\infty}^{\infty}\int_{-\infty}^{\infty} |A|^2 \,\mathrm{d}X\,\mathrm{d}Z. \tag{3.11}$$

According to (3.10), the mean term A_0 decays algebraically at infinity and, taking into account (3.3), so do the lump tails:

$$\eta \sim -\epsilon^2 \frac{I_0}{4\pi}\frac{\partial}{\partial Z}\left(\frac{Z}{X^2+Z^2}\right). \tag{3.12}$$

Finally, inserting the computed locally confined solution of the Davey–Stewartson equations (3.4) and (3.5) in the expansion (3.3), it follows that, for values of γ slightly below the bifurcation point $\gamma_0 = 1$, the peak amplitude η_0 of a lump is given by

$$\eta_0 = \pm\sqrt{2}(1-\gamma)^{1/2}A(0,0) + \cdots, \tag{3.13}$$

where $A(0,0) = 2.15$, $+(-)$ corresponding to elevation (depression) lumps.

3.2. *Finite-amplitude lumps*

We now turn our attention to finite-amplitude lump solutions of the steady 2-DB equation (3.1). Recall that elevation and depression solitary waves of the Benjamin

equation also bifurcate at $\gamma = 1$, and the corresponding solution branches are described close to the bifurcation point by an expression similar to (3.13), the only difference being that $A(0, 0) = 2.15$ is replaced by $2\sqrt{2/3} = 1.63$ (Akylas *et al.* 1998). As discussed below, lump solutions in fact follow a bifurcation scenario very similar to that of plane solitary waves, in the finite-amplitude regime as well.

For the purpose of tracking lump-solution branches in the finite-amplitude regime, we used numerical continuation in the parameter γ, employing the weakly nonlinear results of § 3.1 as a first approximation at the starting point, close to $\gamma = 1$. Following a numerical procedure similar to that used earlier for the Davey–Stewartson equations, the steady 2-DB equation (3.1) was discretized by a pseudospectral approximation combined with mapping of the (ξ, z)-plane into a finite square domain. Locally confined solutions of the 2-DB equation obey the constraint (2.9) so this also had to be imposed on the numerical solution, furnishing an additional equation. The resulting system of nonlinear algebraic equations was solved by Newton's method. Details of implementation of the numerical procedure, including the resolution used in each of the runs and convergence checks, are given in the Appendix.

We begin by comparing the numerically computed profiles of lumps to the weakly nonlinear results of § 3.1. Figure 2 shows ξ- and z-cross-sections of elevation and depression lumps for two values of $\gamma = 0.975$ and $\gamma = 0.995$ which, according to (3.2), correspond to $\epsilon^2 = 0.05$ and $\epsilon^2 = 0.01$, respectively. The weakly nonlinear profiles were obtained correct to $O(\epsilon^2)$, by inserting in expansion (3.3) the locally confined solution of the Davey–Stewartson equations for $A(X, Z)$ and $A_0(X, Z)$ computed in § 3.1. As expected, the agreement between the numerical and asymptotic results improves as ϵ^2 is decreased. At the same time, however, it becomes apparent that the weakly nonlinear theory is quantitatively accurate only very close to the bifurcation point.

We next examine the behaviour of the elevation solution branch in the finite-amplitude regime. Figure 3 summarizes the results in a bifurcation diagram, displaying the lump peak amplitude, $\eta_0 \equiv \eta(\xi = 0, z = 0)$, as a function of γ. As γ is decreased from 1, η_0 increases more rapidly than the weakly nonlinear expression (3.13) would suggest, and the lump profile becomes more localized with fewer oscillations along ξ (figure 4*a*, *b*). Finally, at $\gamma = 0$, the familiar lump solution of the KP-I equation is recovered (figure 4*c*).

Even though $\gamma > 0$ in the flow configuration of interest here, the elevation solution branch can be readily continued for negative values of γ (figure 4*d*); the peak amplitude η_0 continues to increases monotonically and eventually approaches a finite limiting value $\eta_0 \approx 15$ as $\gamma \to -\infty$. In this limit, the BDO dispersive term overwhelms the KdV dispersive term, and the 2-DB equation (2.18) reduces to the two-dimensional BDO equation derived by Ablowitz & Segur (1980) for internal waves in deep fluids, but with the BDO and transverse-variation terms having opposite signs, in which case plane BDO solitary waves are unstable to transverse perturbations. This suggests that the two-dimensional BDO equation, like the KP-I equation, admits lump solutions when plane solitary waves happen to be transversely unstable.

Based on the bifurcation diagram in figure 3, elevation lumps behave in a manner entirely analogous to plane elevation solitary waves of the Benjamin equation. As indicated in figure 3, the latter are directly connected to the KdV solitary wave at $\gamma = 0$ (Albert *et al.* 1999; Calvo & Akylas 2003) and, furthermore, they approach the BDO solitary wave as $\gamma \to -\infty$. Quantatively, however, lumps feature significantly higher peak amplitudes than plane solitary waves.

Turning now to the other lump-solution branch that bifurcates at $\gamma = 1$, the bifurcation diagram corresponding to depression lumps is shown in figure 5. Again,

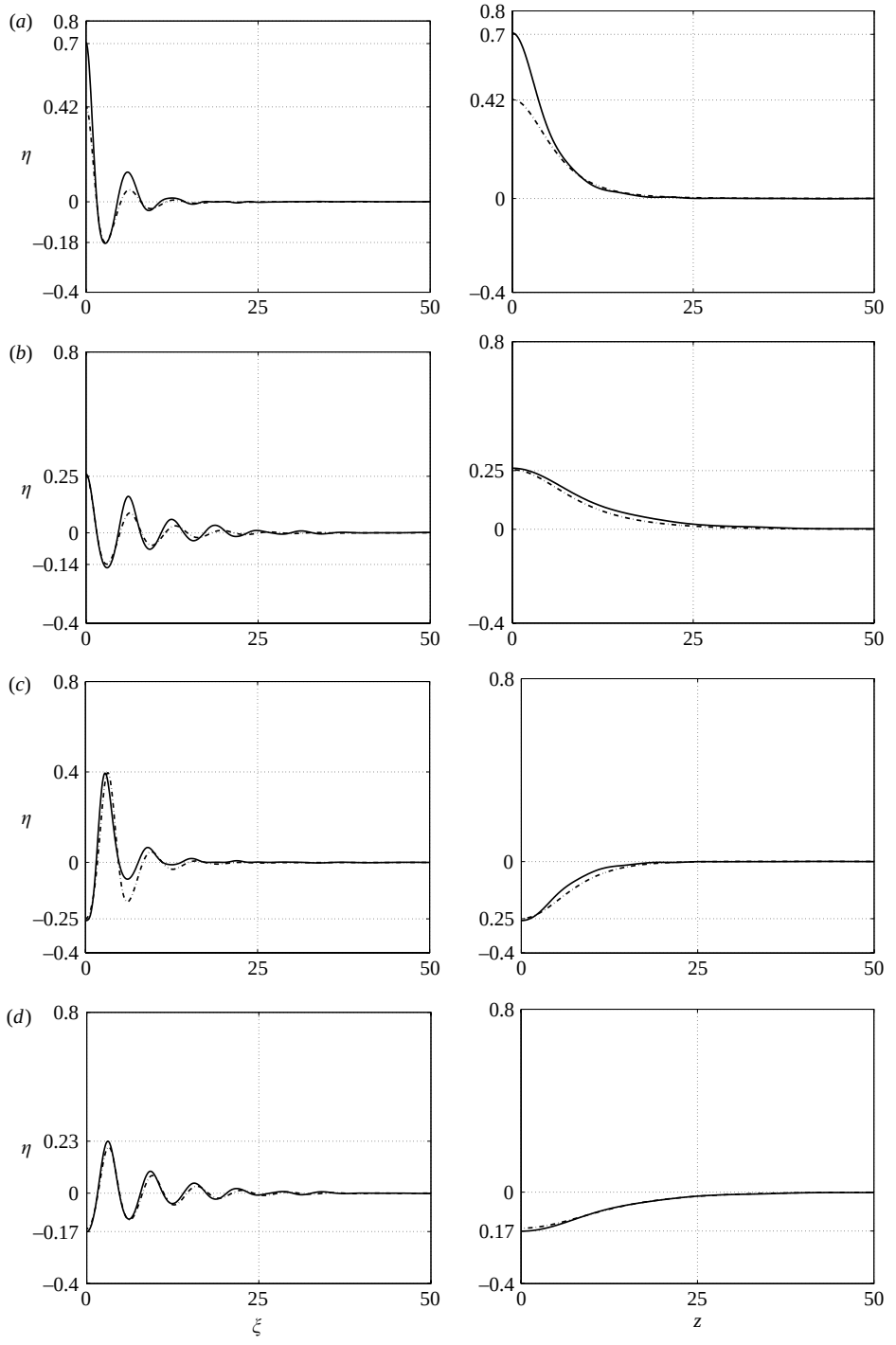

FIGURE 2. Comparison of numerically computed lumps (–) near the bifurcation point to the wavepackets constructed from the weakly nonlinear theory (-·-). Left column: ξ-cross-section, right column: z-cross-section. (a, b) Elevation branch: (a) $2(1-\gamma)=\epsilon^2=0.05$; ($b$) $\epsilon^2=0.01$. (c, d) Depression branch: (c) $\epsilon^2=0.05$; (d) $\epsilon^2=0.01$.

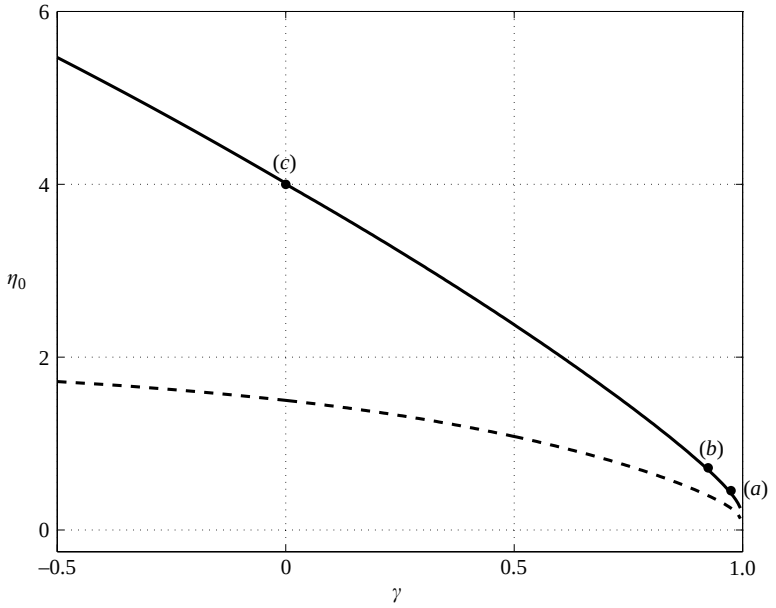

FIGURE 3. Bifurcation diagram of lumps (–) and plane solitary waves (- -) of elevation. The lump profiles corresponding to (*a*), (*b*) and (*c*) are displayed in figure 4.

the value of the profile at the origin, $\eta_0 \equiv \eta(\xi = 0, z = 0)$, which for depression lumps is negative, is plotted as a function of the parameter γ. Here, η_0 does not coincide, in general, with the peak lump amplitude because finite-amplitude depression lumps feature a shallow middle trough and relatively tall side crests (figure 6*a*, *b*). For $\gamma \simeq 0.89$, in fact, a limit point is reached at which the solution branch turns towards increasing values of γ and the middle trough of the lump profile develops a dimple (figure 6*c*, *d*); increasing γ further, the lump profile decreases in amplitude and looks more like two lumps of elevation pieced together in the middle. This behaviour is very similar to that of depression solitary waves of the Benjamin equation (Calvo & Akylas 2003), and the corresponding solution branch is also plotted in figure 5 for comparison.

Although it becomes prohibitively expensive to carry the numerical continuation past the stage shown in figure 5, we expect the branch of depression lumps to turn back towards decreasing values of γ at another turning point very close to 1, and to keep wrapping around, each time getting close to, but never reaching, 1. Such a bifurcation scenario takes place for free-surface gravity–capillary solitary waves of elevation on deep water slightly below the minimum phase speed and the plethora of solitary waves that arises can be interpreted as multi-modal solitary waves (Dias, Menasce & Vanden-Broeck 1996, § 3). The numerical evidence presented in figure 5, although far from complete, hints that the 2-DB equation also admits multi-modal lumps, but here it is the depression branch that behaves like the elevation branch of free-surface solitary waves.

4. Transverse instability

As remarked earlier, in the KdV limit ($\gamma = 0$), the 2-DB equation (2.18) reduces to the so-called KP-I equation, which predicts that plane KdV solitary waves are unstable to transverse perturbations; moreover, the KP-I equation admits lump solutions that

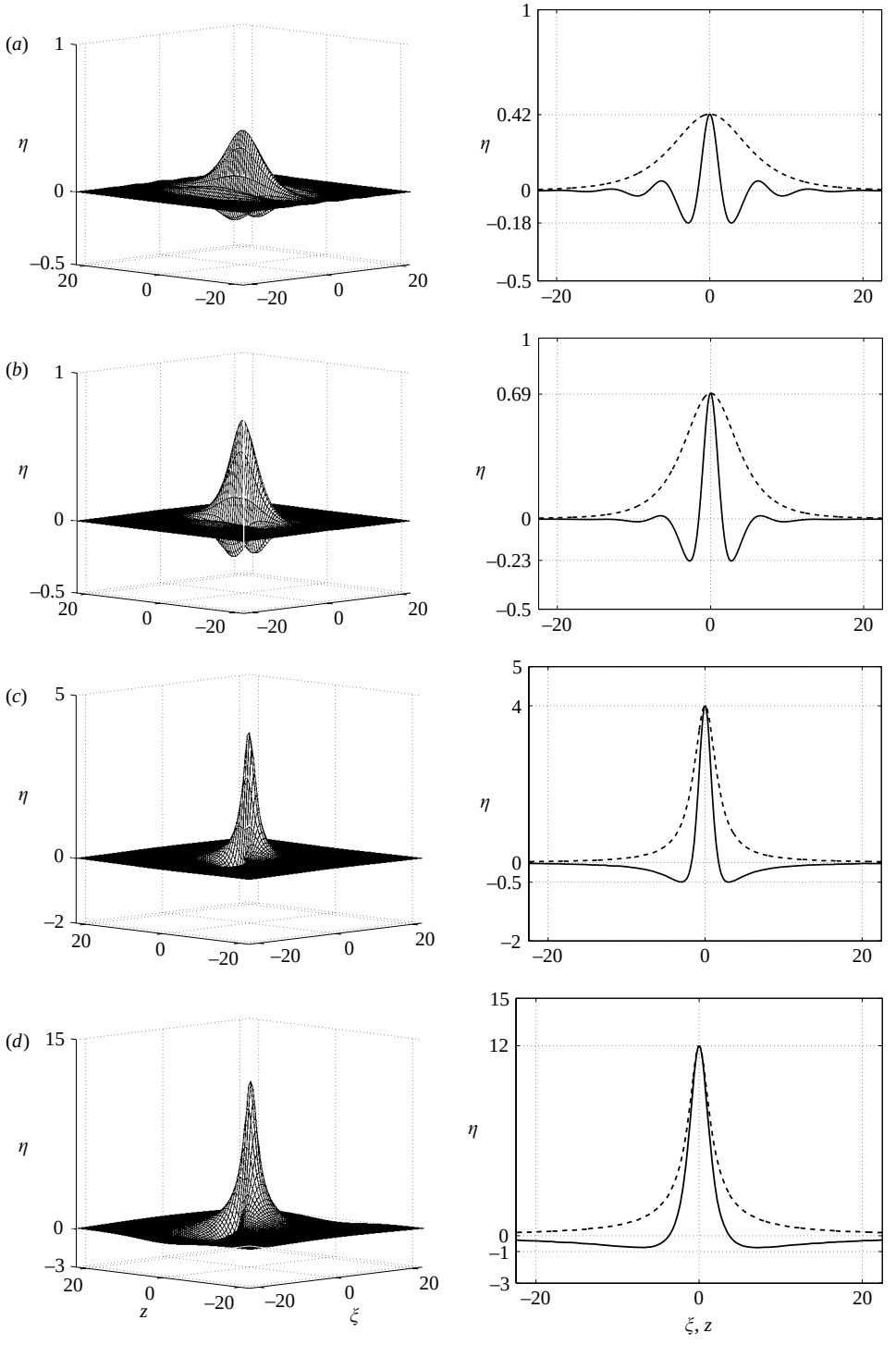

FIGURE 4. Representative lump profiles for the elevation branch. (*a*) $\gamma = 0.975$; (*b*) $\gamma = 0.925$; (*c*) $\gamma = 0$; (*d*) $\gamma = -5$. ξ-cross-section (–), z-cross-section (- -).

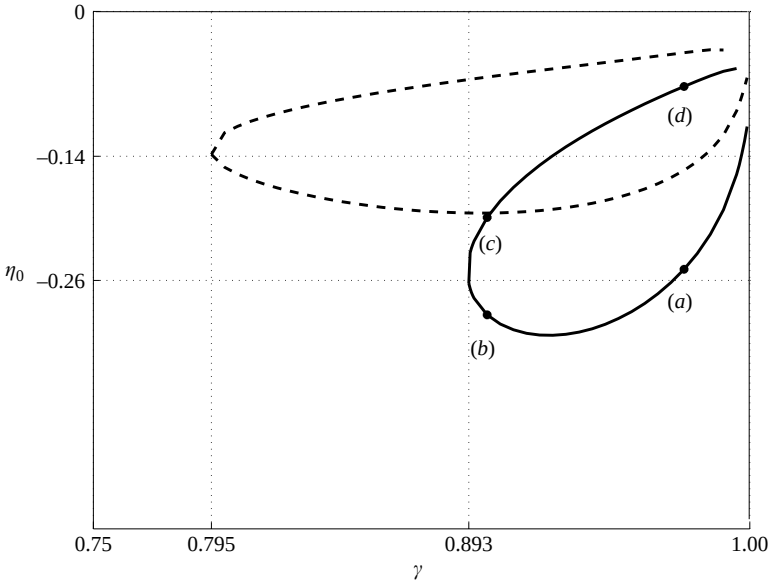

FIGURE 5. Bifurcation diagram of lumps (–) and plane solitary waves (- -) of depression. The lump profiles corresponding to (*a*), (*b*), (*c*) and (*d*) are displayed in figure 6.

become the asymptotic states of the initial-value problem in the presence of transverse variations (Ablowitz & Segur 1979).

The stability of solitary waves of the Benjamin equation to one-dimensional perturbations was explored in Calvo & Akylas (2003). Out of the two solution branches that bifurcate at $\gamma = 1$, the elevation branch turns out to be stable (as was also found by Benjamin 1992) while the depression branch is unstable until the limit point at $\gamma \approx 0.795$ is reached (see figure 5), where an exchange of stabilities is to be expected. While a comprehensive study of the initial-value problem is lacking at present – the Benjamin equation is not integrable – sample numerical solutions suggest that elevation solitary waves can emerge from locally confined initial conditions (Calvo & Akylas 2003).

For the 2-DB equation, the fact that lumps and plane solitary waves of elevation co-exist (see figure 3) would suggest that the latter are unstable to transverse perturbations, as in the analogous case of the KP-I equation noted above. We now proceed to verify this claim based on a perturbation analysis for long transverse disturbances, similar to the one used in Ablowitz & Segur (1980).

Returning to the 2-DB equation (2.18), on the assumption that transverse variations are long, η depends on the stretched coordinate $\hat{Z} = \mu z$, where $\mu \ll 1$:

$$(\eta_t + (\eta^2)_x - 2\gamma \mathscr{H}\{\eta_{xx}\} + \eta_{xxx})_x - \mu^2 \eta_{\hat{Z}\hat{Z}} = 0. \tag{4.1}$$

The leading-order disturbance,

$$\eta = \eta^{(0)}(\xi - \psi(\hat{Z}, \hat{T}); \gamma), \tag{4.2}$$

is assumed to be a plane solitary wave of the Benjamin equation propagating along x with unit speed ($\xi = x - t$) so $\eta^{(0)}$ satisfies

$$-\eta^{(0)} + \eta^{(0)2} - 2\gamma \mathscr{H}\{\eta^{(0)}_\xi\} + \eta^{(0)}_{\xi\xi} = 0; \tag{4.3}$$

the presence of transverse variations in $\eta^{(0)}$ is reflected in the modulated phase ψ

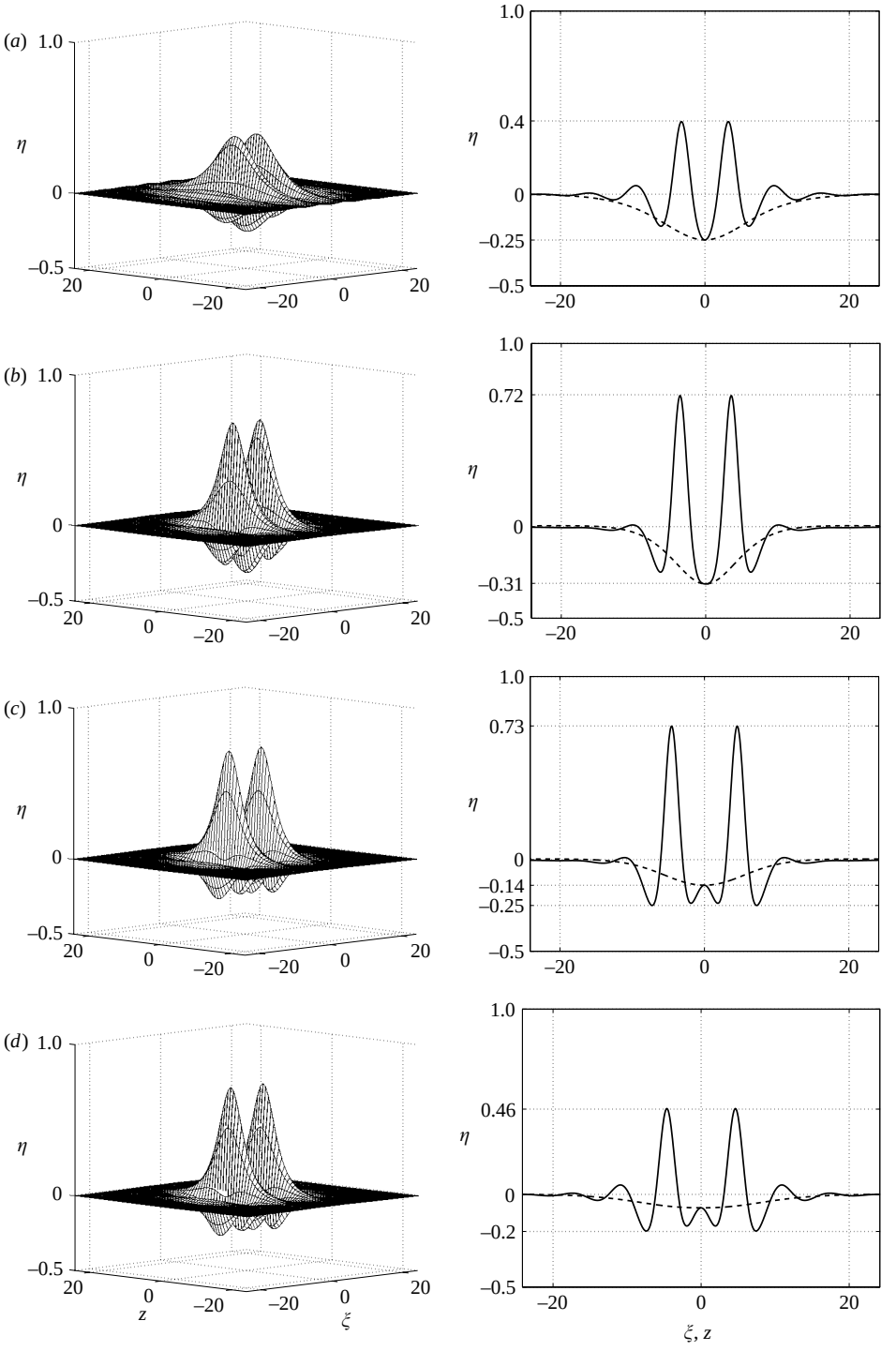

FIGURE 6. Representative lump profiles for the depression branch. (*a*) $\gamma = 0.975$; (*b*) $\gamma = 0.925$; (*c*) $\gamma = 0.925$; (*d*) $\gamma = 0.975$. ξ-cross-section (–), z-cross-section (- -).

that depends on $\hat{Z}$ and the slow time $\hat{T} = \mu t$. The goal of the perturbation stability analysis is to ascertain whether such modulations grow in time.

To this end, upon expanding η in powers of μ,

$$\eta = \eta^{(0)} + \mu\eta^{(1)} + \mu^2\eta^{(2)} + \cdots, \tag{4.4}$$

and substituting in (4.1), it is found that the $O(1)$ equation is already satisfied in view of (4.3). To $O(\mu)$, then, $\eta^{(1)}$ satisfies the forced problem

$$-\eta^{(1)}_{\xi} + 2\big(\eta^{(0)}\eta^{(1)}\big)_{\xi} - 2\gamma\mathscr{H}\big\{\eta^{(1)}_{\xi\xi}\big\} + \eta^{(1)}_{\xi\xi\xi} = -\psi_{\hat{T}}\eta^{(0)}_{\xi} \tag{4.5}$$

or, in short,

$$\mathscr{L}\eta^{(1)} = \mathscr{R}^{(1)}, \tag{4.6}$$

where $\mathscr{L}$ denotes the linear operator on the left-hand side and $\mathscr{R}^{(1)}$ the forcing term on the right-hand side of (4.5).

Invoking now the standard solvability argument, for the forced problem (4.6) to have a locally confined solution, $\mathscr{R}^{(1)}$ must be orthogonal to $\eta^{(0)}$,

$$\int_{-\infty}^{\infty} \mathscr{R}^{(1)}\eta^{(0)}\,\mathrm{d}\xi = 0, \tag{4.7}$$

since $\eta^{(0)}$ is a proper homogeneous solution of the adjoint problem:

$$\mathscr{L}^{+}\eta^{(0)} = \eta^{(0)}_{\xi} - 2\eta^{(0)}\eta^{(0)}_{\xi} + 2\gamma\mathscr{H}\big\{\eta^{(0)}_{\xi\xi}\big\} - \eta^{(0)}_{\xi\xi\xi} = 0, \tag{4.8}$$

in view of (4.3). This solvability condition is trivially met at this order because $\mathscr{R}^{(1)}$ and $\eta^{(0)}$ have opposite parities, and we may readily solve for $\eta^{(1)}$:

$$\eta^{(1)} = \psi_{\hat{T}}\left(\eta^{(0)} + \frac{1}{2}\xi\eta^{(0)}_{\xi} - \frac{1}{2}\gamma\frac{\partial\eta^{(0)}}{\partial\gamma}\right). \tag{4.9}$$

Proceeding next to $O(\mu^2)$, it is found that $\eta^{(2)}$ satisfies a forced problem of the form (4.6) with $\mathscr{R}^{(1)}$ replaced by

$$\mathscr{R}^{(2)} = -\big(\eta^{(1)^2}\big)_{\xi} - \eta^{(1)}_{\hat{T}} + \int^{\xi} \eta^{(0)}_{\hat{Z}\hat{Z}}\,\mathrm{d}\xi. \tag{4.10}$$

Again, for this problem to have a locally confined solution, $\mathscr{R}^{(2)}$ must be orthogonal to $\eta^{(0)}$ and, since $\mathscr{R}^{(2)}$ now is not odd in ξ, this solvability condition translates into an evolution equation for $\psi(\hat{Z}, \hat{T})$:

$$\frac{1}{4}\left\{3\int_{-\infty}^{\infty}\eta^{(0)^2}\,\mathrm{d}\xi - \gamma\frac{\partial}{\partial\gamma}\int_{-\infty}^{\infty}\eta^{(0)^2}\,\mathrm{d}\xi\right\}\psi_{\hat{T}\hat{T}} + \int_{-\infty}^{\infty}\eta^{(0)^2}\,\mathrm{d}\xi\;\psi_{\hat{Z}\hat{Z}} = 0. \tag{4.11}$$

Based on (4.11), therefore, the plane solitary wave is unstable to long transverse modulations if the coefficient of $\psi_{\hat{T}\hat{T}}$ above happens to be positive:

$$3\int_{-\infty}^{\infty}\eta^{(0)^2}\,\mathrm{d}\xi - \gamma\frac{\partial}{\partial\gamma}\int_{-\infty}^{\infty}\eta^{(0)^2}\,\mathrm{d}\xi > 0. \tag{4.12}$$

It can be verified that if, rather than γ, one chooses the wave speed c, to trace solitary-wave solution branches of the Benjamin equation, so $\eta^{(0)} = \eta^{(0)}(\theta; c)$ with $\theta = x - ct$, (4.12) is equivalent to

$$\frac{\partial}{\partial c}\int_{-\infty}^{\infty}\eta^{(0)^2}\,\mathrm{d}\theta > 0, \tag{4.13}$$

consistent with the transverse-instability condition obtained by Bridges (2001) for solitary-wave solutions of Hamiltonian systems.

In the KdV limit ($\gamma = 0$), (4.12) clearly implies instability, recovering the familiar result for the KP-I equation. In the small-amplitude limit near their bifurcation point ($\gamma \to 1$), on the other hand, solitary waves of the Benjamin equation can be approximated as (Akylas *et al.* 1998)

$$\eta = \pm\frac{2\epsilon}{\sqrt{3}}\operatorname{sech}(\epsilon\xi)\cos\xi + \cdots, \tag{4.14}$$

where $\epsilon^2 = 2(1-\gamma)$; to leading order in ϵ, making use of (4.14), therefore,

$$-\gamma\frac{\partial}{\partial\gamma}\int_{-\infty}^{\infty}\eta^{(0)2}\,\mathrm{d}\xi = \frac{2}{\epsilon}\int_{-\infty}^{\infty}\eta^{(0)}\frac{\partial\eta^{(0)}}{\partial\epsilon}\,\mathrm{d}\xi = \frac{8}{3}\int_{-\infty}^{\infty}\operatorname{sech}^2\epsilon\xi\,\cos^2\xi\,\mathrm{d}\xi > 0, \tag{4.15}$$

so the instability condition (4.12) is met, thus confirming that plane solitary waves are unstable to transverse modulations in this limit as well.

For elevation solitary waves, furthermore, we have checked by numerical means that (4.12) is satisfied, and hence the instability persists, for γ in the whole range of interest, $0 \leqslant \gamma < 1$. The evolution of unstable perturbations in the finite-amplitude regime is discussed below.

5. Numerical simulations

Here we report on unsteady numerical simulations of the 2-DB equation (2.18), in an effort to understand the role that lumps play in the evolution of disturbances in two spatial dimensions.

The numerical method of solution is analogous to the one used in Feng, Kawahara & Mitsui (1999) for the KP-I equation. It employs fast Fourier transform (FFT) in x and z combined with leap-frog time stepping:

$$\frac{\hat\eta^{n+1}-\hat\eta^{n-1}}{2\Delta t} + \mathrm{i}l\mathscr{F}\{(\mathscr{F}^{-1}\{\hat\eta^n\})^2\} + \frac{\mathrm{i}}{3}\omega(\hat\eta^{n+1}+\hat\eta^n+\hat\eta^{n-1}) = 0, \tag{5.1}$$

where $\hat\eta^n \equiv \mathscr{F}\{\eta^n\}$ denotes the Fourier transform in x and z at the nth time step and $\omega = 2\gamma k|k| - k^3 - m^2/k$ is the linear dispersion relation of (2.18). In this semi-implicit scheme, two FFTs are needed per time step and, as shown in Kim (2006), Δt is restricted by a stability condition of the form $\Delta t \leqslant O(\Delta x)$. Moreover, the computational domain must be large enough to avoid reflections from the boundaries.

We now return to the transverse instability of plane solitary waves found in § 4 and follow the unstable disturbances in the finite-amplitude regime. For this purpose, we choose as initial condition

$$\eta(x, z, t=0) = a\bar\eta(ax;\gamma), \tag{5.2}$$

where $\bar\eta(x;\gamma)$ is the profile of a plane solitary wave with unit speed, and

$$a(z) = 1 + 0.1\cos\frac{\pi z}{40} \tag{5.3}$$

is an amplitude function that imposes a periodic perturbation in the transverse direction.

Note that the initial condition (5.2) is such that the 'mass' per unit z,

$$\mathscr{M} = \int_{-\infty}^{\infty}\eta\,\mathrm{d}x, \tag{5.4}$$

is uniform along z, as required by the 2-DB equation (2.18) for disturbances that are locally confined in x and periodic in z. According to (2.18), $\mathscr{M}$ is in fact independent

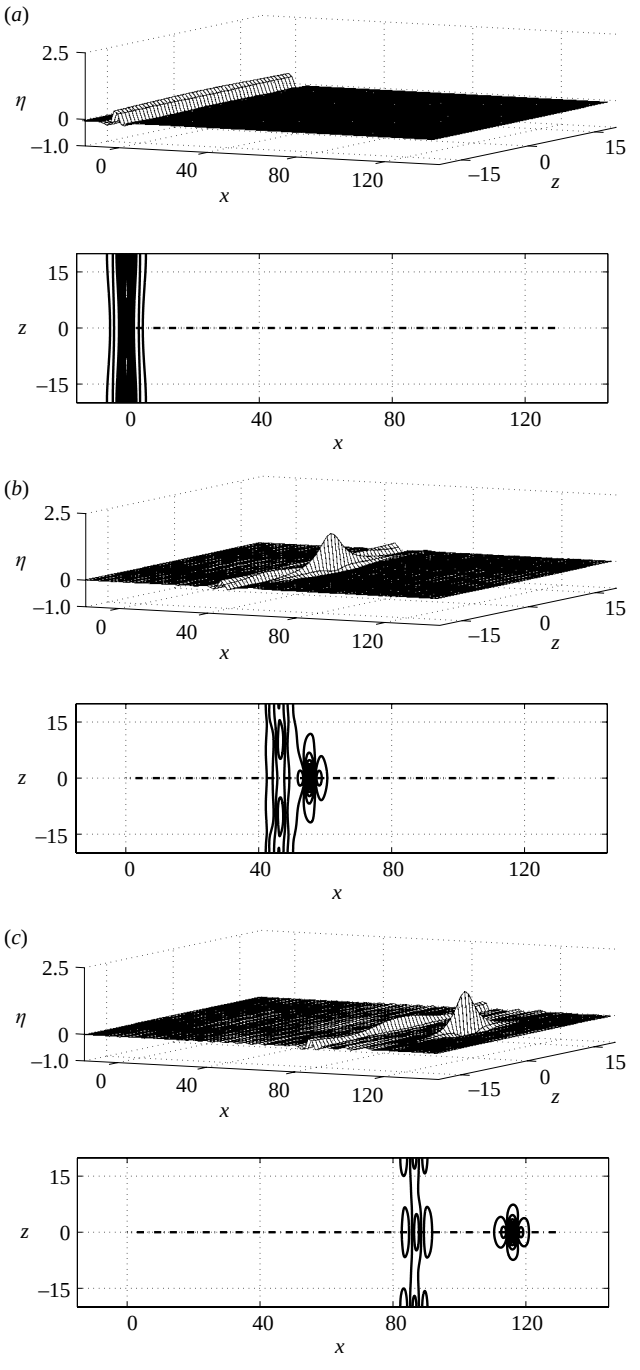

FIGURE 7. Evolution of plane solitary wave of elevation with unit speed (for $\gamma = 0.85$) in the presence of transverse perturbation. (*a*) $t = 0$, (*b*) $t = 50$, (*c*) $t = 100$. An elevation lump with speed $c \approx 1.21$ emerges and propagates ahead of the rest of the disturbance.

of t as well, and this constraint is satisfied exactly by the spectral numerical scheme used here.

Figure 7 shows the initial condition (5.2) corresponding to a plane solitary wave of elevation for $\gamma = 0.85$ and two snapshots of the disturbance at later times. These

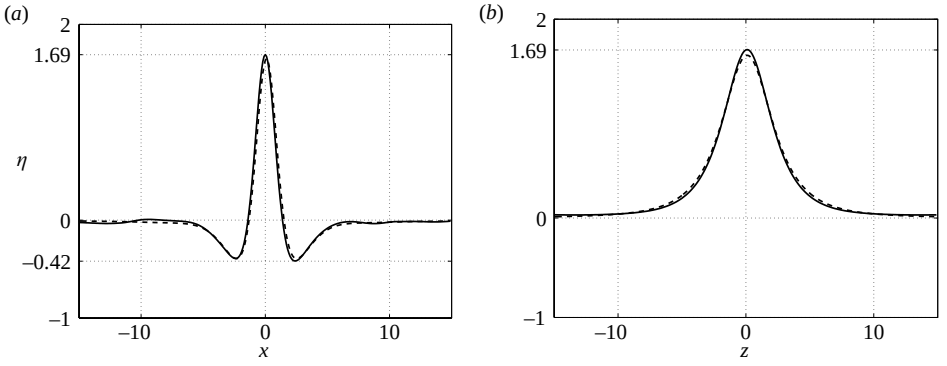

FIGURE 8. Comparison of the upstream-propagating disturbance (–) at $t = 120$, that emerges from the transverse instability of a plane solitary wave $\gamma = 0.85$, to the computed steady elevation lump (- -) propagating with same speed $c \approx 1.21$. (*a*) x-cross-section, (*b*) z-cross-section.

computations were carried out using 1600 Fourier modes in the x-direction and 400 modes in the z-direction with $\Delta x = \Delta z = 0.1$ and $\Delta t = 0.05$. As a result of the transverse instability of the plane solitary wave, a fully localized disturbance resembling a lump of elevation emerges and propagates ahead of the rest of the disturbance with speed $c \approx 1.21$. The profile of the elevation lump having this speed can be readily obtained, via re-scaling

$$x \to \frac{x}{\sqrt{c}}, \quad z \to \frac{z}{c}, \quad \eta \to c\eta, \quad \gamma \to \frac{\gamma}{\sqrt{c}}, \tag{5.5}$$

from the steady lump solutions with unit speed computed in § 3.2, and is compared in figure 8 to the upstream-propagating disturbance found in the unsteady computation at $t = 120$. There is very good agreement between these two profiles, confirming that the localized disturbance arising from the transverse instability of the plane solitary wave is indeed an elevation lump. We also carried out computations with the same initial condition (5.2)–(5.3) but for a solitary wave of larger amplitude ($\gamma = 0.75$), in which case two elevation lumps were shed upstream.

These simulations suggest that the transverse instability of elevation solitary waves results in the formation of elevation lumps which appear to be stable. A comprehensive numerical study of the initial-value problem of the 2-DB equation for locally confined initial conditions, including the interaction of two lumps, is currently under way.

We wish to thank Professors Mark Ablowitz and Victor Shrira for helpful discussions. We are also grateful to the anonymous referees whose comments helped improve the paper significantly. This work was supported by the Air Force Office of Scientific Research, Air Force Materials Command, USAF, under Grant Number FA9950-04-1-0125 and by the National Science Foundation Grant Number DMS-0305940.

Appendix. Computation of finite-amplitude lumps

Here we discuss details of the numerical procedure used for the computation of finite-amplitude steady lumps in § 3.2.

Typically, the profiles of finite-amplitude lumps are such that, while most of the interesting behaviour is localized near the centre, they require a rather large

$N \times M$	$\gamma = 0.5$	$\gamma = 0.75$	$\gamma = 0.975$
128×128	2.3761	1.4465	0.4224
128×96	2.3761	1.4465	0.4224
128×64	2.3761	1.4465	0.4223
96×64	2.3765	1.4468	0.4230

TABLE 1. Convergence of peak amplitude η_0 of elevation lumps as the number of grid points is increased for three values of the parameter γ.

computational domain owing to the algebraic decay at infinity. For this reason, it was decided to use a domain transformation $(\xi, z) \to (p, q)$ that maps the (ξ, z)-plane $(-\infty < \xi < \infty, -\infty < z < \infty)$ into a square $(-1 \leqslant p < 1, -1 \leqslant q \leqslant 1)$:

$$\xi = \frac{Lp}{(1-p^2)^{1/2}}, \quad z = \frac{Lq}{(1-q^2)^{1/2}}, \tag{A 1}$$

L being a scaling factor that was set to $L = 15$. In addition, an uneven collocation mesh, that is clustered near the centre of the wave profile and is relatively coarse in the far field, was used:

$$-1 = p_{2N} < p_{2N-1} < \ldots < p_1 < p_0 = 1, \quad -1 = q_{2M} < q_{2M-1} < \ldots < q_1 < q_0 = 1, \tag{A 2}$$

where $p_n = \cos\theta_{1,n}$ and $q_m = \cos\theta_{2,m}$ with $\theta_{1,n} = n\pi/2N$ and $\theta_{2,m} = m\pi/2M$ $(0 \leqslant n \leqslant 2N, 0 \leqslant m \leqslant 2M)$.

As basis functions, we choose

$$f_n(p) = \frac{1}{a_n} \prod_{\substack{k=0 \\ k \neq n}}^{2N} (p - p_k), \quad a_n = \prod_{\substack{k=0 \\ k \neq n}}^{2N} (p_n - p_k), \tag{A 3}$$

which satisfy $f_n(p_k) = \delta_{nk}$.

The derivative $\partial/\partial p$ then can be represented as a $(2N+1) \times (2N+1)$ matrix:

$$D_{ij} = \frac{1}{a_j} \prod_{\substack{k=0 \\ k \neq i,\, j}}^{2N} (p_i - p_k) = \frac{a_i}{a_j(p_i - p_j)} \quad (i \neq j), \qquad D_{jj} = \sum_{\substack{k=0 \\ k \neq j}}^{2N} (p_j - p_k)^{-1}, \tag{A 4}$$

and likewise $\partial/\partial q$ corresponds to a similar $(2M+1) \times (2M+1)$ differentiation matrix. Owing to the symmetry properties of lumps $\eta(\xi, z) = \eta(\pm\xi, \pm z)$, however, it is possible to reduce the size of these matrices to $(N \times N)$ and $(M \times M)$, respectively, which in turn cuts to $1/16$ the storage memory required for calculating the Jacobian matrix in Newton's iterations.

Finally, the Hilbert transform $\mathscr{H}\{\eta\}$ is computed from (2.8) by quadrature and also results in an $N \times N$ matrix. As discussed in Kim (2006), the treatment of the principal-value integral in (2.8) requires care because of the non-uniform grid used here.

The accuracy of the numerical procedure was tested by monitoring the convergence of the computed lump profiles as the resolution was increased. As a typical example, table 1 illustrates the convergence of the peak amplitude η_0 of elevation lumps for

three values of γ. As expected, higher resolution is required for computing lumps close to the bifurcation point $\gamma = 1$, where the wave profiles resemble wavepackets with several oscillations. The results reported in figures 3–6 were computed using the resolution $N = 128$ and $M = 64$ for which η_0 is converged to four significant figures. Unfortunately, even the higher resolution $N = 128$ and $M = 128$ is not adequate for capturing the second turning point of the depression-lump solution branch, that is expected to occur very close to $\gamma = 1$ (see figure 5).

REFERENCES

Ablowitz, M. J & Segur, H. 1979 On the evolution of packets of water waves. *J. Fluid Mech.* **92**, 691–715.

Ablowitz, M. J & Segur, H. 1980 Long internal waves in fluids of great depth. *Stud. Appl. Maths.* **62**, 249–262.

Ablowitz, M. J. & Wang, X. P. 1997 Initial time layers and Kadomtsev–Petviashvili-type equations. *Stud. Appl. Maths* **98**, 121–137.

Akylas, T. R. 1993 Envelope solitons with stationary crests. *Phys. Fluids* A **5**, 789–791.

Akylas, T. R. 1994 Three-dimensional long water-wave phenomena. *Annu. Rev. Fluid Mech.* **26**, 191–210.

Akylas, T. R. & Dias, F. & Grimshaw, R. H. J. 1998 The effect of the induced mean flow on solitary waves in deep water. *J. Fluid Mech.* **355**, 317–328.

Albert, J. P., Bona, J. L. & Restrepo, J. M. 1999 Solitary-wave solutions of the Benjamin equation. *SIAM J. Appl. Maths* **59**, 2139–2161.

Benjamin, T. B. 1992 A new kind of solitary wave. *J. Fluid Mech.* **245**, 401–411.

Bridges, T. J. 2001 Transverse instability of solitary-wave states of the water-wave problem. *J. Fluid Mech.* **439**, 255–278.

Calvo, D. C. & Akylas, T. R 2003 On interfacial gravity–capillary solitary waves of the Benjamin type and their stability. *Phys. Fluids* **15**, 1261–1270.

Dias, F. & Iooss, G. 1993 Capillary–gravity solitary waves with damped oscillations. *Physica* D **65**, 399–423.

Dias, F., Menasce, D. & Vanden-Broeck J.-M. 1996 Numerical study of capillary–gravity solitary waves. *Eur. J. Mech.* B **15**, 17–36.

Feng, B. F., Kawahara, T. & Mitsui, T. 1999 A conservative spectral method for several two-dimensional nonlinear wave equations *J. Comput. Phys.* **153**, 467–487.

Grimshaw, R. & Melville, W. K. 1989 On the derivation of the modified Kadomtsev–Petviashvilli equation *Stud. Appl. Maths* **80**, 183–202.

Groves, M. D. & Sun, S. M. 2005 Fully localised solitary-wave solutions of the three-dimensional gravity–capillary water-wave problem, preprint.

Katsis, C. & Akylas T. R. 1987 Solitary internal waves in a rotating channel: a numerical study. *Phys. Fluids* **30**, 297–301.

Kim, B. 2006 Three-dimensional solitary waves in dispersive wave systems. Doctoral dissertation, Department of Mathematics, MIT.

Kim, B. & Akylas, T. R. 2005 On gravity–capillary lumps. *J. Fluid Mech.* **540**, 337–351.

Longuet-Higgins, M. S. 1993 Capillary–gravity waves of solitary type and envelope solitons on deep water. *J. Fluid Mech.* **252**, 703–711.

Milewski, P. A. 2005 Three-dimensional localized solitary gravity–capillary waves. *Commun. Math. Sci.* **3**, 89–99.

Papanicolaou, G. C., Sulem, G. C., Sulem, P. L. & Wang, X. P. 1994 The focusing singularity of the Davey–Stewartson equations for gravity–capillary surface waves. *Physica* D **72**, 61–68.

Parau, E., Vanden-Broeck, J.-M & Cooker, M. J. 2005 Nonlinear three-dimensional gravity–capillary solitary waves. *J. Fluid Mech.* **536**, 99–105.